

Unit Commitment Framework for Nuclear Reactors with Reactivity Decline

Shiny Choudhury*, Michael Davidson*[†], George Tynan*

*Mechanical and Aerospace Engineering, University of California, San Diego, CA, USA

[†]School of Global Policy and Strategy, University of California, San Diego, CA, USA

Abstract—Nuclear reactors are often modeled as inflexible, baseload generators with fixed downtimes and restrictive ramping limits. In practice, however, a reactor’s operational flexibility is closely tied to its fuel cycle stage and the associated reactivity margin. A key physical constraint to power maneuverability is *xenon poisoning*, caused by an increase in neutron absorbing xenon concentration following a power ramp down. This can delay or even prevent subsequent power ramp up due to suppressed core reactivity. Additionally, if a reactor is shutdown during periods of low reactivity, restart times can vary significantly due to these xenon transients, leading to longer downtimes. This work introduces a physics informed, metaheuristic modeling approach that embeds fuel cycle dynamics directly with a unit commitment (UC) framework. The framework tracks reactivity margin, dynamically activates xenon related constraints, and endogenously implements refueling outages based on the core conditions. By capturing intra-cycle reactivity evolution and the conditional onset of xenon poisoning, the formulation allows for operation dependent nuclear dispatch that reflects both regulatory limits and physical behavior. When applied to a representative reactor fleet operating in distinct modes of operation—ranging from baseload to part load—the framework reveals that flexible operation can slow reactivity degradation and extend fuel cycles. The results show that fuel cycle aware flexibility modeling is critical for accurate scheduling of nuclear reactors and offers a tractable pathway to integrate nuclear power in energy system models.

I. INTRODUCTION

Nuclear power plants (NPPs) have traditionally been among the most inflexible thermal generators, but now face tremendous pressure to operate more flexibly due to the rapid integration of variable renewable energy (VRE) into electric grids [1]. As VRE penetration grows, so does the variability of net load curves, placing increasing demands on conventional generators to provide ramping capability, part load operation, and fast startup/shutdown services [2]–[6]. Since VRE increasingly sets marginal prices, NPPs must depart from their historical “must-run” operational modes and engage in levels of cycling and modulation rarely required in the past [7]. This shift challenges both the physical capabilities and economic assumptions that have traditionally underpinned nuclear operations, demanding a more dynamic framework for scheduling and system integration.

Despite these changing operational demands, large scale power system models continue to represent NPPs as inflexible baseload units governed by static, single valued parameters [8]. However, in reality, nuclear reactors exhibit fuel cycle

dependent flexibility. For much of the fuel cycle, reactors can operate flexibly in response to grid signals, but as they approach the end of the cycle, core physics introduces additional binding constraints. These arise from the accumulation of fission fragments and neutron poisons (such as xenon-135) in the control rods, leading to higher minimum power levels and longer downtime after a shutdown [9], [10].

While a growing body of literature has started recognizing the importance of incorporating nuclear reactor physics and fuel cycle effects into power system models, most studies still assume limited or infrequent cycling of reactors, and treat operational constraints as fixed throughout the simulation horizon [7], [11]–[13]. As a result, most models decouple power output from the evolving physical state of the core. This abstraction carries significant consequences: because nuclear fuel is stored onboard, prolonged low capacity factor operation (as demanded in VRE-heavy mixes) extends the cycle length and postpones the onset of reactivity limiting conditions [14]. And static NPP model’s fail to capture this relationship.

This study addresses the modeling gap by introducing a physics informed unit commitment framework that explicitly links core reactivity margin, resulting xenon transient, and economic dispatch. Thus enabling a realistic representation of NPP behavior across different operational modes while capturing physical constraints. To the authors’ knowledge, this is the first tractable formulation that embeds full cycle nuclear physics in a unit commitment setting. By modeling these dynamic feedbacks, the framework moves beyond static constraint formulations and provides a stronger basis for assessing the role of NPPs in VRE dominated grids and otherwise.

II. FRAMEWORK

Nuclear reactors operate under a complex set of constraints stemming from regulatory requirements, engineering design limits, and the fundamental physics of fission reaction. Operational constraints such as ramp rates, minimum generation levels, and downtime durations are typically imposed exogenously during standard dispatch [8], [15]. For example, in the United States, an AP1000 reactor is typically permitted to reduce power from 100% to 50% and return to full power only once within a 24-hour window [16]. However, as the reactor progresses through its fuel cycle, physics driven constraints—such as increasing minimum generation levels and longer downtime begin to apply. These constraints introduce

a strong temporal dependence and reflect the evolving core reactivity margins. In this study, we first derive these physics induced constraints as a function of fuel cycle progression and encode them into a precomputed lookup table. This table is then used to dynamically enforce reactor level operational limits during the dispatch of a nuclear fleet under different operational modes within a high-VRE energy mix.

The widely deployed Westinghouse AP1000 Pressurized Water Reactor (PWR) serves as the reference technology for illustration of the formalism in this study [16]. The AP1000 has a net electrical output of approximately 1000 MWe, and it's primary loop uses pressurized water as both coolant and neutron moderator. Heat from this loop is transferred to a secondary circuit that operates on a Rankine cycle, driving a turbine to generate electricity. The reactor core is composed of fuel assemblies arranged in a 17×17 lattice, using low-enriched uranium dioxide (UO₂) with enrichment levels up to 5% U-235. Core reactivity is controlled via a combination of black and grey control rods made of boron carbide (B₄C), actuated through the control rod drive mechanism (CRDM) [17]. The remainder of this paper is organized as follows:

- Section III-A investigates core reactivity under various power ramping scenarios, focusing on the introduction of negative reactivity during xenon poisoning
- Section III-B presents a reactivity margin degradation model adapted for flexible reactor power output
- Section III-C derives reactivity dependent operational parameters, including limits on minimum generation level and downtime following a reactor shutdown
- Section IV integrates these constraints in a modified Unit Commitment (UC) formalism, embedding fuel cycle tracking. This section introduces novel constraints to the canonical UC model for nuclear representation
- Section V presents the overall metaheuristic dispatch formalism in a structured pseudocode

III. DETERMINATION OF REACTIVITY DEPENDENT PARAMETERS

A. Xenon poisoning and negative reactivity

During a power ramp down in a nuclear reactor, the concentration of xenon (¹³⁵Xe) increases due to the radioactive decay of iodine (¹³⁵I), a fission product. ¹³⁵Xe is a potent neutron absorber, and its concentration continues to rise for several hours after a ramp down has concluded [10]. Within the reactor core, maintaining criticality requires a precise neutron balance, which ¹³⁵Xe disrupts. This effect, known as *xenon poisoning*, reduces the core reactivity and temporarily limits the reactor's ability to ramp power back up.

Equation (1) and Equation (2) describe the one point differential equations governing the evolution of ¹³⁵I and ¹³⁵Xe concentrations as a function of core neutron flux [10]. The time varying neutron flux, $\phi(t)$, is modeled proportional to the power transition as shown in Equation (3).

$$\frac{d^{135}\text{I}(t)}{dt} = -\lambda_I^{135}\text{I}(t) + \gamma_I \phi(t) \bar{\Sigma}_f \quad (1)$$

$$\begin{aligned} \frac{d^{135}\text{Xe}(t)}{dt} &= \lambda_I^{135}\text{I}(t) - \lambda_{Xe}^{135}\text{Xe}(t) \\ &\quad + \gamma_{Xe} \phi(t) \bar{\Sigma}_f - \sigma_{abs}^{Xe} \phi(t) ^{135}\text{Xe}(t) \end{aligned} \quad (2)$$

$$\phi(t) = \phi_0 \times \left(\frac{P(t)}{P_0} \right) \quad (3)$$

Steady state concentrations of ¹³⁵I and ¹³⁵Xe are obtained by setting the time derivatives in Equation (1) and Equation (2) to zero and solving for ¹³⁵I_{eq} and ¹³⁵Xe_{eq}, respectively. The derived expressions are shown in Equation (4) and Equation (5).

$$^{135}\text{I}_{eq} = \frac{\gamma_I \phi_0 \bar{\Sigma}_f}{\lambda_I} \quad (4)$$

$$^{135}\text{Xe}_{eq} = \frac{\phi_0 \bar{\Sigma}_f (\gamma_I + \gamma_{Xe})}{\lambda_{Xe} + \sigma_{abs}^{Xe} \phi_0} \quad (5)$$

¹³⁵Xe absorbs fission neutrons and introduces a negative reactivity within the core (also referred to as 'Xenon defect') that is computed using Equation (6).

$$\rho_{Xe}(t) \approx \frac{\sigma_{abs}^{Xe} ^{135}\text{Xe}(t)}{v \bar{\Sigma}_f} \quad (6)$$

In Figure 1, the evolution of ¹³⁵I, ¹³⁵Xe, and the resulting xenon defect in four distinct power ramp scenarios are shown. All the parameters in the equations above are for the AP1000 reactor and summarized in Table V [9], [11].

During a power ramp down, the ¹³⁵Xe concentration transiently increases due to ¹³⁵I decay before eventually decreasing and equilibrating (Figure 1a). Conversely, during a power ramp up, ¹³⁵Xe concentration initially decreases before stabilizing at a new higher equilibrium value corresponding to the higher power level (Figure 1b). The resulting xenon defect in both these ramping scenarios follow the trend of ¹³⁵Xe evolution. We also simulate a power ramp up immediately following a power ramp down event (Figure 1c), and a ramp down following a ramp up event (Figure 1d). In both cases, the peak xenon defect is smaller in magnitude than the isolated ramp down, and it stabilizes more quickly. In this study we want to avoid xenon defect induced power stagnation altogether, hence we are interested in the peak values of the xenon defect in various ramping events. This peak eventually depends on (1) the power level before the ramp down begins and (2) the depth of the power reduction or the ΔP [9]–[11].

B. Core reactivity margin with flexible power output

In PWRs, flexibility can be realized by ramping core power or by venting steam before it reaches the turbine [18]. Core ramping is typically performed using control rods or by varying the boron concentration in the coolant (referred to as *chemical shim*) [9]. The control rod assembly includes a combination of highly absorbing 'black rods' and partially absorbing 'grey rods', each characterized by different neutron absorption cross-sections. By controlling the insertion and withdrawal of these rods, operators can regulate neutron flux and thereby control reactor power. Over time, however,

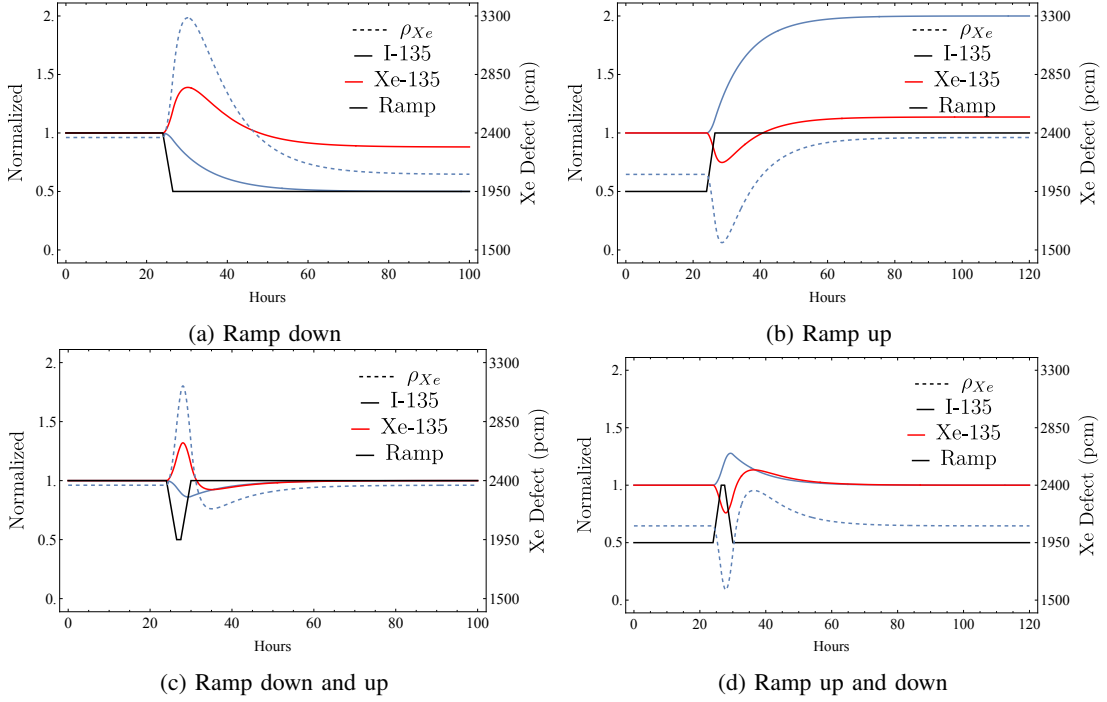


Fig. 1: ^{135}Xe , ^{135}I and Xenon defect evolution in 4 different ramp scenarios

neutron absorbing fission products accumulate within the fuel rods, reducing core reactivity margin and narrowing the range of achievable power maneuvers [11]. During these periods, a severe case of xenon poisoning can lead to power stagnation for several hours.

Consequently, the operational flexibility achievable at any given time is a balance between the core reactivity margin (determined by the operational history of the fuel) and the gradually increasing negative reactivity during large power ramp downs. To quantify the core reactivity, we use the effective multiplication factor, k_{eff} , that measures the ratio of the neutron population from one generation to the next. When a reactor has fresh fuel, $k_{eff} > 1$ so that criticality can be maintained in the face of fuel burn up and other losses. At steady state, an instantaneous $k_{eff} = 1$ is maintained at all times by the use of control rods and/or chemical shims [9]. The core reactivity margin, which represents the reactor's ability to overcome xenon poisoning, is computed using the k_{eff} at different stages of the fuel cycle (indexed by n) as shown in Equation (7).

$$\Delta\rho_{\text{margin},n} = \frac{k_{\text{eff},n} - 1}{k_{\text{eff},n}} \times 10^5 \text{ [pcm]} \quad (7)$$

Reactivity is typically expressed in pcm (per cent mille), where $1 \text{ pcm} = 1 \times 10^{-5}$. It is important to note that the value $k_{eff,n}$ is the multiplication factor in the absence of control rod and chemical shim and thus takes value ≥ 1 . The parameter $k_{eff,n}$ starts at an initial value at beginning-of-life (BOL), denoted $k_{eff,BOL}$, and gradually degrades as fissile nuclei are consumed, eventually approaching a minimum of $k_{eff,n} \simeq 1$, at which point the reactor must undergo refueling.

For nuclear reactors, fuel burnup quantifies the cumulative

energy extracted from the nuclear fuel over time. It is a useful metric because a freshly fueled PWR core contains enough fissile material to support a range of burnup trajectories, depending on the reactor's time-varying capacity factor during operation. At full power operation, the reactor undergoes maximum burnup and the degradation rate, m is known from empirical observations [9]. During flexible power output, k_{eff} degradation will be dictated by the degree of part load operation, which will then be reflected in the burnup levels.

To model this relationship, we define a simple recursive relation in Equation (8), where the degradation rate m is scaled by the capacity factor α_n to compute the effective multiplication factor $k_{eff,n+1}$ from $k_{eff,n}$. The capacity factor α_n (defined in Equation (9)), is the ratio of actual generation to the theoretical maximum over period T . The updated value $k_{eff,n+1}$ is then used to calculate the remaining reactivity margin, which directly affects the reactor's operational flexibility in period $n + 1$.

$$k_{\text{eff},n+1} = k_{\text{eff},n} - m * \alpha_n \quad (8)$$

$$\alpha_n = \frac{\sum_{t=1}^T P_t}{P_{\text{max}} \times T} \quad (9)$$

C. Reactivity margin dependent parameters

As a reactor reaches low reactivity levels due to fuel burnup, limits on allowable ramps begin to apply. The minimum generation levels gradually increases until the reactor can offer no ramping without a power stagnation [7], [9], [11]. Additionally, longer downtime start applying in case of a shutdown [10]. In the following section we compute these parameters

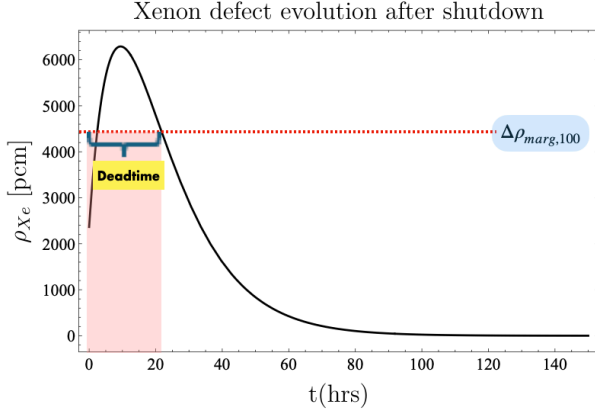


Fig. 2: Deadtime determination for an illustrative xenon defect evolution resulting from full power operation to shutdown. The value depends on the reactivity margin remaining in the core and is a variable.

which are then used as inputs in a Unit Commitment (UC) model.

1) *Minimum generation level*: To maximize operational flexibility, xenon poisoning induced power stagnation needs to be avoided at all reactivity levels. As a result, the minimum generation level accessible increases slowly dependent on stage of the fuel cycle. To compute these minimum generation levels, we start by defining a piecewise ramp down from full power (P_{\max}) to a parameterized value P_0 at a ramp rate of 25%/hr, shown in Equation (10) [8]. n_0 is the hour at which the ramp down ends.

$$\frac{P_t}{P_{\max}} = \begin{cases} 1, & t = 0 \\ 1 - 0.25t, & 0 < t \leq n_0 \\ P_0/P_{\max}, & t > n_0 \end{cases} \quad (10)$$

This piecewise ramp down function is used to approximate the neutron flux in the core using Equation (3), which is then used to compute the xenon defect evolution via Equation (6). The peak xenon defect value, denoted as $\rho_{Xe,\max}(P_0)$, is evaluated for a range of power ramp down from full power operation to P_0 values and stored in a lookup table. For a given stage in the fuel cycle n , the minimum allowable generation level or $P_{\min,n}^*$ is determined based on the remaining core reactivity margin, $\Delta\rho_{\text{marg},n}$, as defined in Equation (11). $P_{\min,n}^*$ represents the lowest generation level that can be reached from full power through the maximum permissible ramp rate without inducing xenon poisoning induced power stagnation.

$$P_{\min,n}^* = \arg \min_{P_0} |\Delta\rho_{\text{marg},n} - \rho_{Xe,\max}(P_0)| \quad (11)$$

s.t. $\Delta\rho_{\text{marg},n} - \rho_{Xe,\max}(P_0) > 0$

2) *Deadtime after shutdown*: In rare instances, a reactor may need to shutdown when the core reactivity is low. Such a shutdown can be treated as a power ramp down to zero and introduces additional constraints for subsequent restart. In this case, without an ongoing neutron flux, the ^{135}Xe concentration transiently increases to even higher peaks since there are

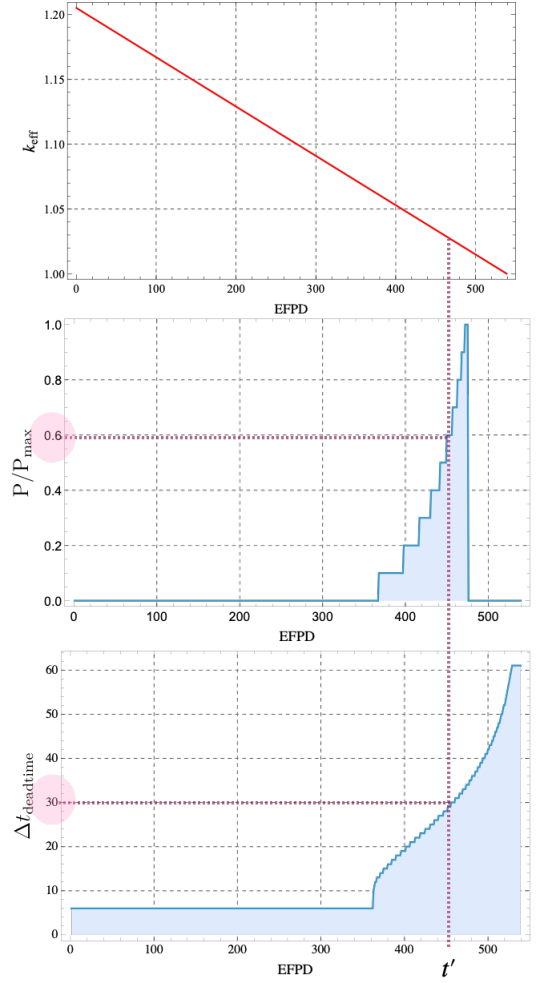


Fig. 3: Determination of exogenously set P_{\min} and Deadtime value based on the core reactivity before short term UC dispatch.

no active ^{135}Xe sinks [10]. To safely restart the reactor, a mandatory downtime—referred to as *deadtime*—must be observed to allow for substantial ^{135}Xe to decay. The duration of this deadtime, denoted by $\Delta t_{\text{deadtime},n}$, is defined as the time interval following a shutdown after which the xenon defect or $\rho_{Xe}(t)$ is strictly less than the available reactivity margin, $\Delta\rho_{\text{marg},n}$ and decreasing. After this period, the reactor may safely restart without violating core reactivity constraints. Assuming a full power to zero shutdown, the deadtime computation is given by Equation (12).

$$\Delta t_{\text{deadtime},n} = \sup \{t \in \mathbb{R}^+ \mid \rho_{Xe}(t) > \Delta\rho_{\text{marg},n}\} \quad (12)$$

Figure 2 illustrates the evolution of the xenon defect following a shutdown from full-power operation, the available reactivity margin on day 100, and the resulting deadtime that the reactor must observe before restart is feasible. In the shown figure, the deadtime is at least 22 hours, after which the core has enough excess reactivity to manage the xenon defect and permit a restart. A precomputed deadtime value table is derived using Equation (12) for various reactivity margins which is

then used as input for the UC.

Exhaustive xenon kinetics simulations for several ramp protocols were performed to generate a lookup table that links minimum allowable power level ($P_{\min,n}^*$) and post shutdown deadtime ($\Delta t_{\text{deadtime},n}$) to the remaining reactivity margin. Figure 3 illustrates pictorially the lookup table parameters enforcement across different k_{eff} values as the fuel undergoes burnup. In effect, we adjust reactivity degradation based on reactor operation at full load or part load by scaling degradation based on burnup. This allows us to track reactivity decline over time, impose appropriate operating constraints, and prevent power stagnation. In the next section we discuss the use of these parameters in a UC framework.

IV. UNIT COMMITMENT WITH REACTIVITY TRACKING

Power plants operate under a range of technical constraints such as ramp up/down rates, minimum up and down times, and startup/shutdown durations—all of which must be considered when scheduling a heterogeneous fleet of generators. Unit Commitment (UC) is a mixed integer linear programming (MILP) formulation widely used for this purpose [19]. The UC model determines the optimal commitment or on/off status and generation levels for individual generators to minimize total operational cost while satisfying all technical constraints. Commitment schedules are communicated to plant operators in advance, and uncertainties in demand or renewable generation are handled by incorporating reserve margins into the schedule [20]. We modify the UC model to serve as a subproblem within a reactivity tracking wrapper, enabling realistic representation of nuclear power plant operation.

A. Objective function

The objective of the Unit Commitment (UC) formulation includes the canonical components: variable generation cost, startup cost, and a penalty for non-served energy (NSE). Additionally, a shutdown cost term is included to capture the operational costs associated with shutting down nuclear reactors, as motivated in [8]. The complete objective function is defined in Equation (13).

$$\begin{aligned} \min \sum_{g \in G} C_{\text{var},g} \cdot p_{g,t} + \sum_{t \in T} C_{\text{nse}} \cdot \text{nse}_t \\ + \sum_{g \in G_{\text{nuc}}} \sum_{t \in T} (C_{\text{start},g} \cdot z_{g,t}^{\text{start}} + C_{\text{shut},g} \cdot z_{g,t}^{\text{shut}}) \end{aligned} \quad (13)$$

B. Unit commitment constraints

For discrete commitment of thermal generators, we use the three variable startup, shutdown and commit constraints [21]. The generators are constrained by to minimum power levels, ramp rates, uptime and downtime. Additionally, we introduce two key changes for nuclear reactor representation—a variable minimum power level and downtime/deadtime based on remaining reactivity margins. Equation (14) to Equation (18) summarize the commitment constraints that discretely enforce minimum generation level and downtime on all thermal generators, including nuclear reactors. $z_{g,h}^{\text{on}}, z_{g,h}^{\text{start}}, z_{g,h}^{\text{shut}} \in \{0, 1\}$ are

binary variables representing the commitment status, startup, and shutdown actions, respectively.

$$p_{g,t} \geq P_{g,n}^{\min} \times z_{g,t}^{\text{on}} \quad \forall g \in G_{\text{nuc}}, t \in T \quad (14)$$

$$p_{g,t} \leq P_g^{\max} \times z_{g,t}^{\text{on}} \quad \forall g \in G_{\text{nuc}}, t \in T \quad (15)$$

$$z_{g,t}^{\text{on}} \geq \sum_{t'=t-\text{MinUp}_g}^t z_{g,t'}^{\text{start}} \quad \forall g \in G_{\text{nuc}}, t \in T \quad (16)$$

$$1 - z_{g,t}^{\text{on}} \geq \sum_{t'=t-\text{MinDn}_{g,n}}^t z_{g,t'}^{\text{shut}} \quad \forall g \in G_{\text{nuc}}, t \in T \quad (17)$$

$$z_{g,t+1}^{\text{on}} - z_{g,t}^{\text{on}} = z_{g,t+1}^{\text{start}} - z_{g,t+1}^{\text{shut}} \quad \forall g \in G_{\text{nuc}}, t \in T-1 \quad (18)$$

Typically, nuclear reactors are exogenously constrained to operate within a limited power range due to economic or regulatory requirements. Hence, the generation from each reactor at each time period must stay within $p_{g,h} \in [P_{g,n}^{\min}, P_{\max}]$ where the minimum generation level, $P_{g,n}^{\min}$ for each $g \in G_{\text{nuc}}$ is defined as:

$$P_{g,n}^{\min} = \max(P_{\min,\text{base}}, P_{\min,n}^*)$$

Here, $P_{\min,\text{base}}$ is an exogenously set minimum generation level, while $P_{\min,n}^*$ is the level determined by the remaining reactivity margin on day n as computed in Section III-C1. Similarly, the minimum downtime for each reactor is defined as:

$$\text{MinDn}_{g,n} = \max(\text{MinDn}_{\text{base}}, \Delta t_{\text{deadtime},n})$$

where $\text{MinDn}_{\text{base}}$ is the baseline downtime dictated by mechanical wear, Rankine cycle inertia, and safety protocols, and $\Delta t_{\text{deadtime},n}$ accounts for xenon-induced deadtime, also precomputed based on reactivity levels on day n as computed in Section III-C2.

TABLE I: Illustrative state transitions for minimum stable time implementation with $\Delta t_{\text{stable}} = 2$.

t	z_t^{on}	up_t	rd_t	st_t	Description
0	1	0	0	1	Initial steady-state generation
1	1	0	1	0	Ramp-down begins
2	1	0	1	0	Ramp-down continues
3	1	0	0	1	Stability period enforced
4	1	0	0	1	Stability period enforced
5	1	1	0	0	Ramp-up begins
6	1	1	0	0	Ramp-up continues
7	1	0	0	1	Return to stable generation
8	0	0	0	0	Reactor shut down

C. Minimum stable time constraints

Following a power ramp down, nuclear reactors are required to maintain a stable power level for a minimum duration before they can ramp power again. This is to allow operators to manage core conditions while accounting for xenon transients [16]. We begin by introducing three binary variables

$rd_{g,t}$, $st_{g,t}$, $up_{g,t} \in \{0, 1\}$, defined for each reactor $g \in G_{\text{nuc}}$ and time step $t \in T$, as originally formulated by Jenkins et al. [7]. The variable $rd_{g,t}$ serves as a ramp down indicator and is activated (i.e., transitions from 0 to 1) when a ramp down occurs between $t-1$ and t . Similarly, $up_{g,t}$ indicates a ramp up over the same interval. Both ramp down and ramp up events are defined by a threshold change in generation by δ , as captured in Equation (20) and Equation (22).

$$p_{g,t}^{aux} = p_{g,t} - P_{g,n}^{\min} \times z_{g,t}^{on} \quad (19)$$

$$p_{g,t+1}^{aux} - p_{g,t}^{aux} \geq \delta - M \times (1 - up_{g,t}) \quad (20)$$

$$p_{g,t+1}^{aux} - p_{g,t}^{aux} \leq up_{g,t} \times \text{RampUp}_g \quad (21)$$

$$p_{g,t}^{aux} - p_{g,t+1}^{aux} \geq \delta - M \times (1 - rd_{g,t}) \quad (22)$$

$$p_{g,t}^{aux} - p_{g,t+1}^{aux} \leq rd_{g,t} \times \text{RampDn}_g \quad (23)$$

$$st_{g,t+k} \geq rd_{g,t} - rd_{g,t+1} \quad \text{for all } t \in [1, T - \Delta t_{\text{stable}} - 1], \quad (24)$$

$$k \in [1, \Delta t_{\text{stable}}],$$

$$g \in G_{\text{nuc}} \quad rd_{g,t} + up_{g,t} + st_{g,t} = z_{g,t}^{on} \quad \forall g \in G_{\text{nuc}}, t \in T \quad (25)$$

When a ramp down ends or specifically, when $rd_{g,t-1} = 1$ and $rd_{g,t} = 0$, the stable state indicator $st_{g,t}$ is activated, requiring the reactor to remain at a constant generation level for Δt_{stable} hours before the next power ramp up is allowed. Finally, the sum of the three binary variables $rd_{g,t}$, $up_{g,t}$, $st_{g,t}$ must equal 1 at each time step, and these binaries are only active when a unit is committed, i.e., $z_{g,t}^{on} = 1$. Equation (19)–Equation (25) formalizes this logic and summarize the constraints. In Table I state transition of the binary variables for an illustrative ramping scenario with a stability duration of $\Delta t_{\text{stable}} = 2$ hours is illustrated.

V. FRAMEWORK ALGORITHM

Algorithm 1 summarizes the complete formalism for short term unit commitment (UC) dispatch of a nuclear reactor fleet with the reactivity tracking wrapper. Each scenario begins by initializing the fresh fuel multiplication factors, $k_{\text{eff},\text{BOL}}$, for each reactor. The UC subproblem then determines the hourly generation $p_{g,h}$, from which the capacity factor α_0 for the first period is computed. This feeds into the recursive relation in Equation (8), which updates the reactivity margin using Equation (7) prior to the next dispatch window. The resulting value of $\Delta \rho_{\text{marg},1}$ is used to adjust the minimum generation levels $P_{g,1}^{\min}$ and downtime durations $\text{MinDn}_{g,1}$ via the previously developed lookup tables. This iterative process is repeated for each period n .

Once a reactor reaches the refueling threshold ($k_{\text{eff}} \simeq 1$), it undergoes an outage for a fixed duration Δt_{refuel} . In this study, we assume $\Delta t_{\text{refuel}} = 35$ days, consistent with the average refueling outage duration for large PWRs in the United States in 2024 [22]. During refueling, the reactor is offline and unavailable for generation, leading the UC model to incur non served energy (NSE). After the outage, the reactor restarts with a fresh fuel assembly, and the multiplication factor is reset to $k_{\text{eff},\text{BOL}}$. This sequence—dispatch, reactivity degradation,

Algorithm 1: Modified Unit Commitment with Reactivity Tracking

Input: $k_{\text{BOL},g}$, P_g^{\min} , downtime lookup tables, Δt_{refuel}

Output: $p_{g,t} \quad \forall g \in G_{\text{nuc}}, t \in T$

foreach $g \in G_{\text{nuc}}$ **do**

$k_{0,g} \leftarrow k_{\text{BOL},g};$
 $\tau_g \leftarrow 0$

for $n = 1$ **to** N **do**

foreach $g \in G_{\text{nuc}}$ **do**

if $k_{n,g} \leq 1$ **and** $\tau_g = 0$ **then**

$\tau_g \leftarrow \Delta t_{\text{refuel}}$

if $\tau_g > 0$ **then**

 Set $p_{g,t} \leftarrow 0$ for all $t \in T$;

$\tau_g \leftarrow \tau_g - 1$;

if $\tau_g = 0$ **then**

$k_{n,g} \leftarrow k_{\text{BOL},g}$

continue;

$\Delta \rho_{g,n}^{\text{marg}} \leftarrow \frac{1 - k_{n,g}}{k_{n,g}} \cdot 10^5$;

 Retrieve $P_{g,n}^{\min}$ and $\text{MinDn}_{g,n}$ from lookup table using $\Delta \rho_{g,n}^{\text{marg}}$;

 Solve short-term UC subproblem;

foreach $g \in G_{\text{nuc}}$ **do**

$\alpha_{n,g} \leftarrow \frac{\sum_{t \in T} p_{g,t}}{|T| \cdot P_g^{\max}}$;

$k_{n+1,g} \leftarrow k_{n,g} - m \cdot \alpha_{n,g}$;

operational constraint update, and refueling—repeats across multiple fuel cycles, forming a closed loop feedback between economic dispatch decisions and nuclear physics constraints.

VI. CASE STUDY

A. Basic Setup

To demonstrate the proposed formulation, we simulate the dispatch of a nuclear reactor fleet alongside a VRE-dominant resource mix to meet demand in the ERCOT South Central load zone [23]. Hourly demand data for this zone, as well as ERCOT-wide hourly wind and solar generation profiles for the years 2021–2023, were obtained from publicly available datasets [24]. Monthly installed capacities of wind and solar resources were used to compute hourly capacity factors for variable renewable energy (VRE).

A simplified capacity expansion model (CEM) was solved to determine the optimal installed capacities of wind, solar, and short-duration energy storage for the load zone. These capacities serve as fixed inputs to the modified unit commitment (UC) model. While the proposed framework is fully convex and can be extended to incorporate transmission constraints, the UC model is solved without network modeling in this case study to preserve clarity of exposition. Table II summarizes the optimal capacities obtained from the CEM and the cost assumptions used. Nuclear fleet cost parameters are based on the estimates provided by Stauff et al. [8]. Figure 4 presents the hourly demand, net load, and rolling average statistics to

illustrate the temporal variability that the nuclear fleet must accommodate within the South Central load zone.

TABLE II: Input table for modified UC formalism

Tech	Capacity (GW)	Variable Cost (\$/MWh)	Start/Shut Cost (\$/MW)
Nuclear	4.0	2.8	107.68
Wind	10.0	0	—
Solar	4.0	0	—
Storage	4.2 (4-hr)	0	—

As mentioned earlier, nuclear reactors operate within a complex set of constraints that are exogenously set [8], [15]. And as a reactor progresses through its fuel cycle, additional constraints come into effect based on the reactivity margins. Consequently, the physics induced constraints are a function of the operational strategies and introduce a strong temporal coupling. In this study we endogenize the physics constraints and operate the reactors in different modes, as summarized in Table III.

TABLE III: Modes of operation and parameter definition

Scenario id	Min Gen (%)	Ramp Rate (%/hr)	Notes
Mode-1	100%	—	Must run at full power or shutdown
Mode-2	50%	25%	Can ramp down to 50% Min Gen
Mode-3	20%	25%	Can ramp down to 20% Min Gen

Mode-1 represents the traditional baseload operation of nuclear reactors, where the fleet can only startup or shutdown entire units to load follow. In contrast, Mode-2 and Mode-3 allow reactors to operate at reduced generation values, with hourly ramping levels constrained by predefined ramp up/down rates [8]. These operational modes influence both the dispatchability of the fleet and the rate at which declining reactivity margin inflexibilities emerge, ultimately affecting the onset and frequency of refueling outages.

The UC formalism is solved over a 3 year dispatch horizon with rolling 3 day (72-hour) subproblems, with commitment states transferred at subproblem boundaries. The choice of a 3 day window is made to ensure that the longest xenon induced deadtime is contained within a single rolling horizon. The minimum stable time (Δt_{stable}) is assumed to be 6 hours, which is equal to the base minimum downtime ($\text{MinDn}_{\text{base}}$). The minimum uptime is set to 4 hours. For modeling reactivity degradation in the 3 day dispatch intervals, the 24 hour full power degradation rate m is scaled by a factor of 3, i.e., total degradation per subproblem is approximated as $3m$.

All simulations were performed on an Apple M1 MacBook with 64 GB of RAM. The optimization model is solved using

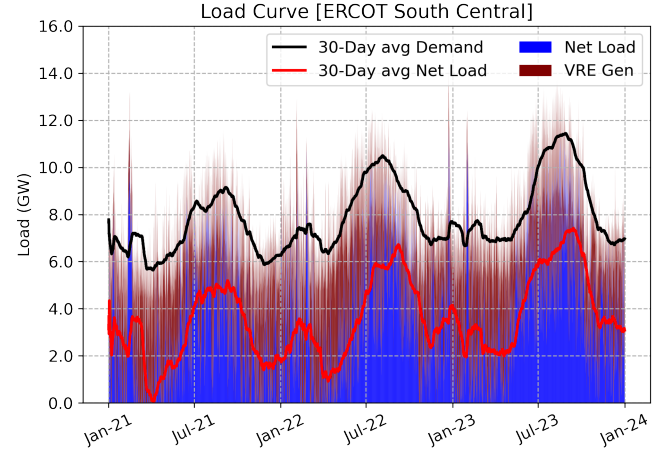


Fig. 4: ERCOT South Central load statistics

the Gurobi solver with MIP gap of 0.1%. Gurobi's presolve and parallelism features were enabled to accelerate convergence.

B. Results

To discuss the strength of the formulation, various dispatchability metrics must be compared holistically across the operational modes. We focus on VRE curtailment, non served energy (NSE) as a percent of demand and energy production costs.

1) *Dispatchability metrics:* Table IV summarizes the percentage of VRE curtailment and NSE accumulated over three years of dispatch. We observe the lowest curtailment in Mode-3, where individual reactors can ramp down to the lowest minimum generation levels. This increased flexibility allows the fleet to accommodate more of the available VRE. Conversely, Mode-1 exhibits the highest curtailment due to its restrictive operation, where reactors can only startup or shutdown entirely. This can be clearly seen in the illustrative 3 day dispatch stackplot is shown in Figure 5. Mode-1 is poorly suited to follow the net load variability and keeps all units online to avoid accumulating startup/shutdown costs. Mode-1 also drives more use of the available storage in the absence of other meaningful flexibility actions. In Mode-3, most of the available VRE penetrates dispatch as the individual reactors can access very low generation levels.

TABLE IV: Scenario description table with operational parameters for both reactor fleets.

Scenario id	NSE (%)	VRE Curt (%)	Cost (mn\$)
Mode-1	5.8%	20.3%	930
Mode-2	5.2%	7.5%	760
Mode-3	2.6%	2.9%	699

Since we model multiple fuel cycles, NSE has two components-1) operational NSE and 2) refueling outage NSE.

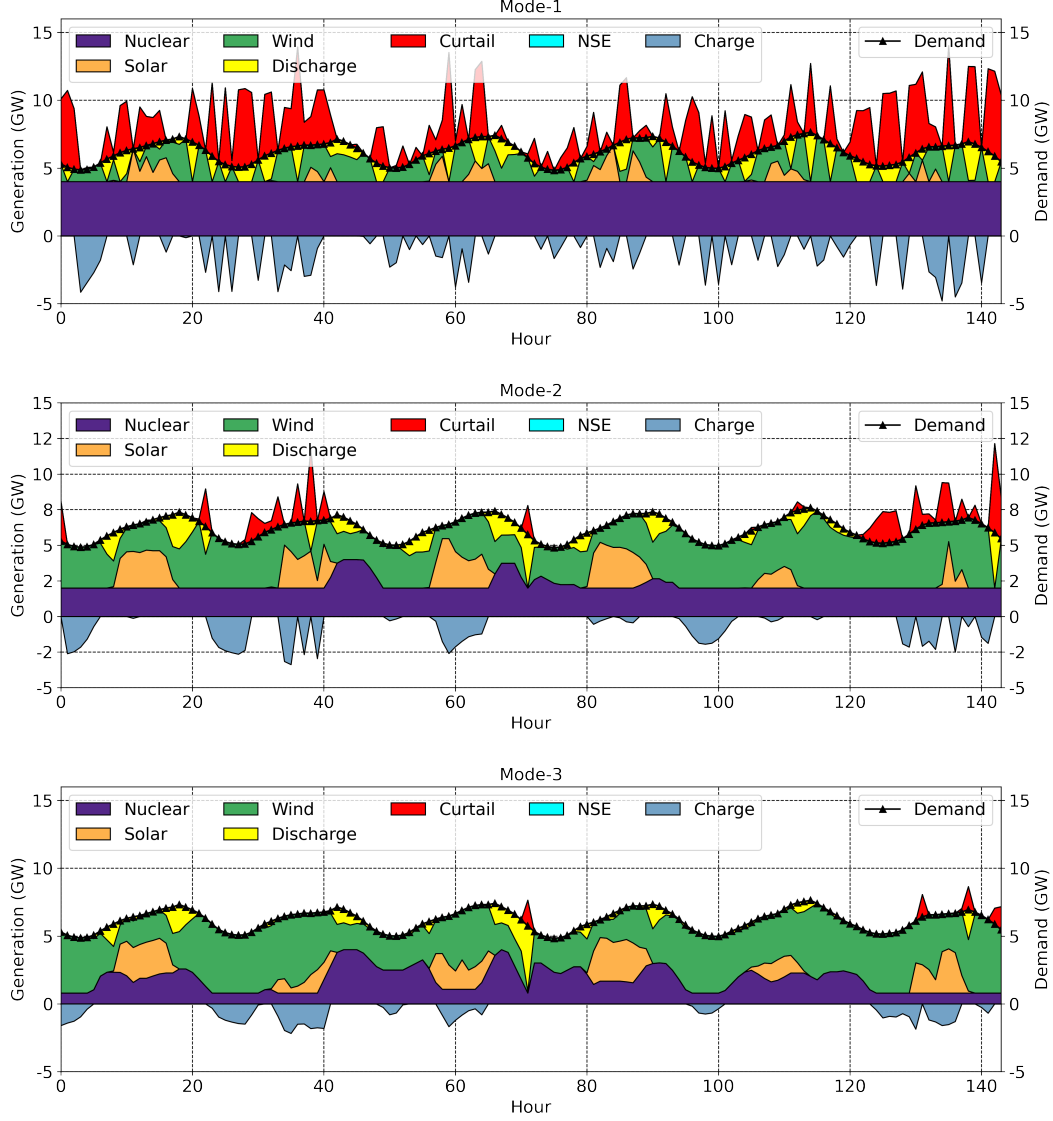


Fig. 5: Illustrative energy dispatch stackplot and demand for different modes of operation

The later accumulates when reactors are offline due to refueling outages. While in reality, energy shortfalls during refueling would be covered by external sources (e.g., imports or backup generators), our model highlights the structural impact of refueling on dispatchability. In Mode-1, the operational NSE are elevated indicating that the fleet fails to adjust flexibly during normal operations and accumulates significant unmet load. In Mode-2 and Mode-3, the fleet reduces NSE by strategic cycling of its fleet to balance reducing unmet load and maximize VRE penetration. These trends are further reflected in total operational costs. Mode-3 exhibits the lowest production cost, benefiting from increased VRE penetration and reduced startup/shutdown cycling. In contrast, Mode-1 incurs highest cost due to more frequent cycling and inefficient dispatch.

2) *Fuel cycle impacts:* Figure 6. summarizes the capacity factor (α_n) evolution for individual reactors across the dispatch period. These trends illustrate how reactor generation is

affected as k_{eff} approaches critical thresholds, leading to longer downtimes and higher minimum generation constraints. We observe that Mode-1 results in the earliest onset of refueling, followed by Mode-2 and then Mode-3. This trend aligns with expected capacity factor behavior: reactors in Mode-1 operate at consistently high output, accelerating fuel burnup and reactivity degradation. We observe the first refueling event around month 18 in Mode-1, consistent with the typical refueling cycle of a Westinghouse AP1000 [16]. We also observe the second onset of inflexibilities in this mode around year 3. This benchmarks our model and proves the ability of our formalism to capture real world reactor behavior.

In contrast, reactivity degrades more slowly in Mode-2 and Mode-3, delaying the onset of refueling. These results are consistent with findings by Alhadhrami et al., who reported that flexible and staggered operation extends refueling intervals [14]. Our formalism captures this behavior by adapting refueling dynamics based on the operational modes. Across all

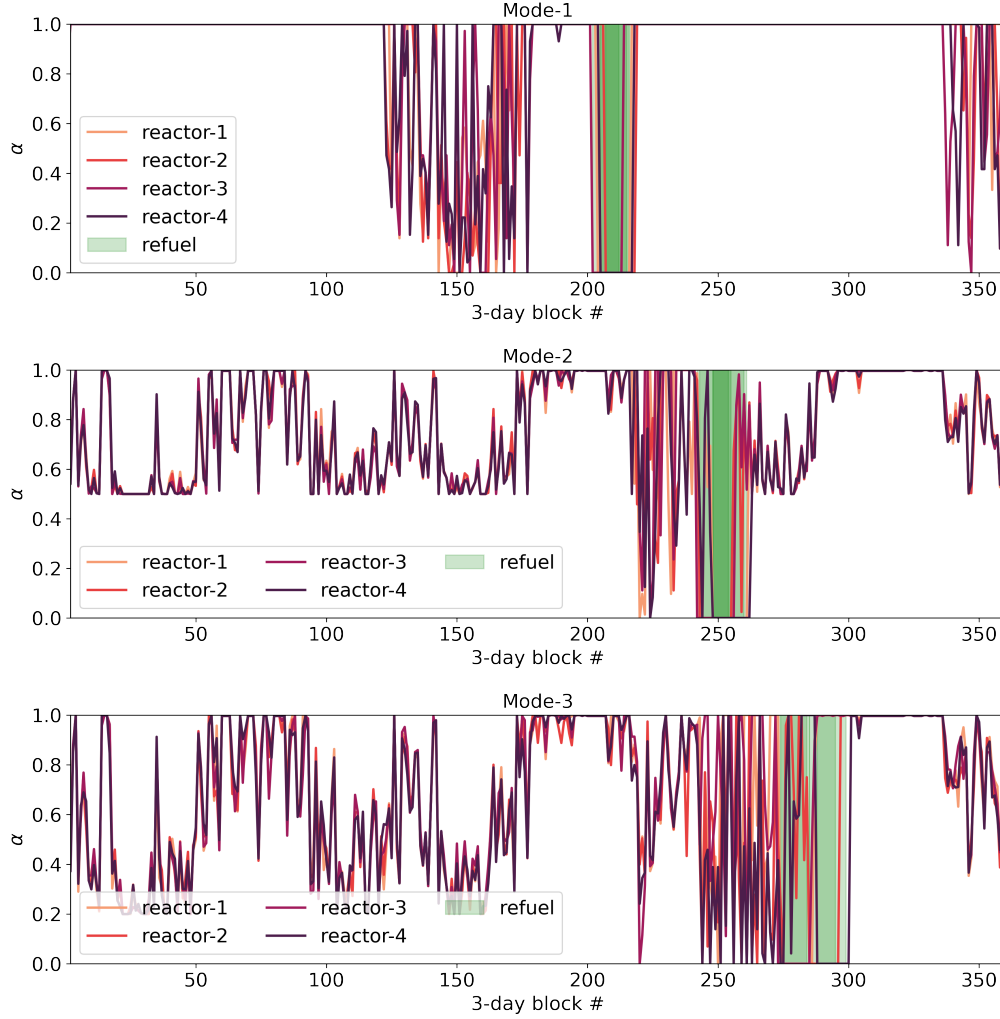


Fig. 6: α evolution of nuclear fleet in different operational modes across 3 year dispatch period

modes, we observe increased cycling of reactors near refueling outages. This occurs because individual units become less flexible as they approach end-of-cycle conditions, and the only remaining source of fleet level flexibility is through startup and shutdown of entire units. This period is also marked by especially elevated NSE values.

Figure 7 highlights the evolution of $P_{g,n}^{\min}$ across the fleet in Mode-2 and Mode-3 for each reactor. As reactivity margins degrade, P_{\min} values escalate to higher values, reducing operational flexibility. Within the fleet however, reactors can cycle between more and less flexible units to delay individual refueling events. However, once a reactor reaches a P_{\min} of 100%, it effectively becomes inflexible, operating like a Mode-1 unit but incurring longer downtimes when shutdown.

With more flexible reactor operation, refueling outages are expected to become longer and more distributed over time. We observe this behavior in Figure 6, where Mode-3 shows a spread out refueling of the fleet. However, since reactor scheduling is primarily driven by economic factors, commitment and dispatch decisions will ultimately depend on the market and energy mix. In particular, the renewed demand growth driven by AI and data center loads may

incentivize more flexible nuclear operation—especially when capital costs are absorbed by data center operators deploying nuclear alongside VRE. In such a setting, nuclear flexibility is likely to be actively leveraged to enhance reliability and enable extended refueling cycles.

VII. CONCLUSION

Most energy system models represent nuclear reactors with fixed, inflexible operational constraints, thereby underestimating their potential flexibility. In reality, a reactor's constraints are tightly coupled to its fuel cycle and associated reactivity margins. For much of the cycle, reactors can respond flexibly to grid signals; however, as they near end-of-cycle, core physics imposes additional binding constraints. These stem from the buildup of fission products, gradual degradation of control rod worth, and xenon poisoning—particularly following a power ramp down, which suppresses core reactivity and induces power stagnation. To capture this, we develop lookup tables that encode maneuverability limits by increasing minimum generation levels and enforcing extended downtimes as a function of the reactor's core state. These tables are used to augment the canonical unit commitment constraints,

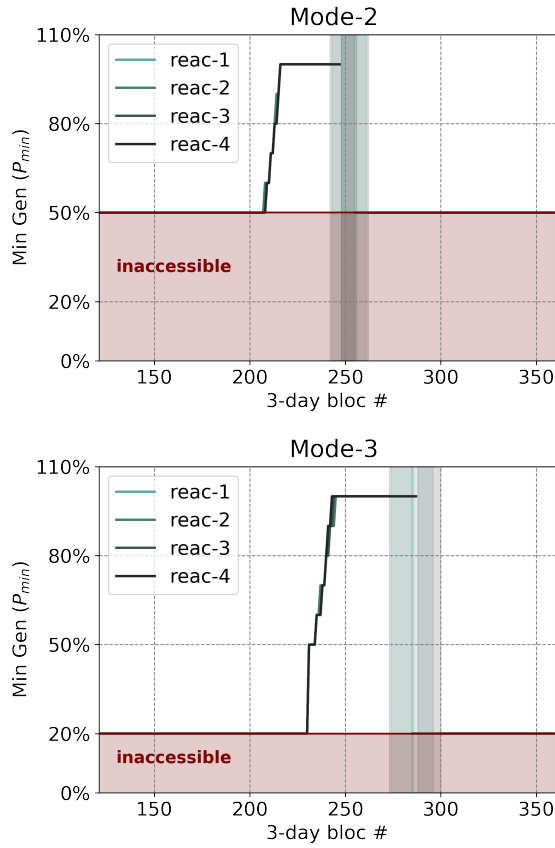


Fig. 7: Minimum generation evolution for Mode-2 and Mode-3 operation after year 2 of dispatch.

allowing for a more accurate representation of nuclear reactor operation. In effect this study introduces a novel formulation that integrates reactivity degradation, core state dependent operational constraints update, refueling and economic dispatch within a unit commitment framework spanning multiple fuel cycles.

Using this framework, we dispatch a fleet of large nuclear reactors under three distinct operational modes within a VRE-heavy energy mix. Mode-1 reflects traditional baseload operation, where the fleet can only follow load by starting up or shutting down entire units. In contrast, Mode-2 and Mode-3 enable part load operation, allowing reactors to reduce power adhering to predefined ramp rates. These flexible modes reduce both VRE curtailment and non-served energy at lower production costs. Mode-1 results in the highest production cost, the greatest VRE curtailment, and the largest accumulation of non-served energy. Moreover, we find that flexible operation, as in Mode-2 and Mode-3, slows reactivity degradation and delays both xenon induced inflexibilities and the onset of refueling outages. The modeling approach dynamically updates core dependent constraints using metaheuristic lookup tables, enabling the capture of intra cycle reactivity evolution, xenon poisoning, and restart delays. Overall, this work generalizes nuclear reactor representation in energy system models and provides a physics informed, computationally tractable formalism for reflecting both regulatory limits and reactor physics in

operational scheduling.

VIII. ACKNOWLEDGMENTS

The authors acknowledge Professor Dennis G. Whyte for many insightful discussions. We thank Zhenhua Zhang, Jenny Nicolas and, Kaarthi A. Gnapathy for their valuable feedback at various stages of this work. Finally, we acknowledge Dr. Namit Anand for insights on how ‘theoretical physicists think about technology’.

APPENDIX

TABLE V: Key Parameters for Westinghouse AP1000

Parameter	Value
Average neutron flux, ϕ_0	1.8×10^{17} n/cm ² ·hr
Macroscopic fission cross-section, $\bar{\Sigma}_f$	0.39497 cm ⁻¹
Iodine decay constant, λ_I	0.01033 hr ⁻¹
Xenon decay constant, λ_{Xe}	0.0753 hr ⁻¹
Iodine effective yield, γ_I	0.0639
Xenon effective yield, γ_{Xe}	0.00237
Xenon microscopic absorption cross-section, σ_{abs}^{Xe}	2.65×10^{-18} cm ²
Neutrons per fission, ν	2.42

REFERENCES

- [1] G. Haratyk, "Early nuclear retirements in deregulated U.S. markets: Causes, implications and policy options," *Energy Policy*, vol. 110, pp. 150–166, Nov. 2017. [Online]. Available: <https://linkinghub.elsevier.com/retrieve/pii/S0301421517305177>
- [2] S. Impram, S. Varbak Nese, and B. Oral, "Challenges of renewable energy penetration on power system flexibility: A survey," *Energy Strategy Reviews*, vol. 31, p. 100539, Sep. 2020. [Online]. Available: <https://www.sciencedirect.com/science/article/pii/S2211467X20300924>
- [3] W.-P. Schill, M. Pahle, and C. Gambardella, "Start-up costs of thermal power plants in markets with increasing shares of variable renewable generation," *Nature Energy*, vol. 2, no. 6, pp. 1–6, Apr. 2017, number: 6 Publisher: Nature Publishing Group. [Online]. Available: <https://www.nature.com/articles/nenergy201750>
- [4] M. A. Gonzalez-Salazar, T. Kirsten, and L. Prchlik, "Review of the operational flexibility and emissions of gas- and coal-fired power plants in a future with growing renewables," *Renewable and Sustainable Energy Reviews*, vol. 82, pp. 1497–1513, Feb. 2018. [Online]. Available: <https://www.sciencedirect.com/science/article/pii/S1364032117309206>
- [5] H. Shaker, H. Zareipour, and D. Wood, "Impacts of large-scale wind and solar power integration on California's net electrical load," *Renewable and Sustainable Energy Reviews*, vol. 58, pp. 761–774, May 2016. [Online]. Available: <https://www.sciencedirect.com/science/article/pii/S1364032115016706>
- [6] P. D. Lund, J. Lindgren, J. Mikkola, and J. Salpakari, "Review of energy system flexibility measures to enable high levels of variable renewable electricity," *Renewable and Sustainable Energy Reviews*, vol. 45, pp. 785–807, May 2015. [Online]. Available: <https://www.sciencedirect.com/science/article/pii/S1364032115000672>
- [7] J. Jenkins, Z. Zhou, R. Ponciroli, R. Vilim, F. Ganda, F. de Sisternes, and A. Botterud, "The benefits of nuclear flexibility in power system operations with renewable energy," *Applied Energy*, vol. 222, pp. 872–884, Jul. 2018. [Online]. Available: <https://linkinghub.elsevier.com/retrieve/pii/S0306261918303180>
- [8] N. Stauff, W. N. Mann, K. Biegel, T. Levin, J. D. Rader, A. Cuadra, and S. H. Kim, "Reactor Power Size Impacts on Nuclear Competitiveness in a Carbon-Constrained Future," Argonne National Lab. (ANL), Argonne, IL (United States), Tech. Rep. ANL/NSE-21/55, Sep. 2021. [Online]. Available: <https://www.osti.gov/biblio/1865640>
- [9] F. Franceschini and B. Petrovic, "Advanced operational strategy for the IRIS reactor: Load follow through mechanical shim (MSHIM)," *Nuclear Engineering and Design*, vol. 238, no. 12, pp. 3240–3252, Dec. 2008. [Online]. Available: <https://www.sciencedirect.com/science/article/pii/S002954930800294X>
- [10] J. R. Lamarsh and A. J. Baratta, *Introduction to nuclear engineering*, 3rd ed., ser. Addison-Wesley series in nuclear science and engineering. Upper Saddle River, N.J: Prentice Hall, 2001.
- [11] R. Ponciroli, Y. Wang, Z. Zhou, A. Botterud, J. Jenkins, R. B. Vilim, and F. Ganda, "Profitability Evaluation of Load-Following Nuclear Units with Physics-Induced Operational Constraints," *Nuclear Technology*, vol. 200, no. 3, pp. 189–207, Dec. 2017. [Online]. Available: <https://www.tandfonline.com/doi/full/10.1080/00295450.2017.1388668>
- [12] J. Rahman and J. Zhang, "Steady-State Modeling of Small Modular Reactors for Multi-Timescale Power System Operations With Temporally Coupled Sub-Models," *IEEE Transactions on Power Systems*, vol. 40, no. 1, pp. 793–805, Jan. 2025. [Online]. Available: <https://ieeexplore.ieee.org/document/10522977/>
- [13] A. Lynch, Y. Perez, S. Gabriel, and G. Mathonniere, "Nuclear fleet flexibility: Modeling and impacts on power systems with renewable energy," *Applied Energy*, vol. 314, p. 118903, May 2022. [Online]. Available: <https://www.sciencedirect.com/science/article/pii/S0306261922003282>
- [14] S. Alhadhrami, G. J. Soto, and B. Lindley, "Dispatch analysis of flexible power operation with multi-unit small modular reactors," *Energy*, vol. 280, p. 128107, Oct. 2023. [Online]. Available: <https://www.sciencedirect.com/science/article/pii/S0360544223015013>
- [15] L. Loflin and B. McRimmon, "Advanced Nuclear Technology: Advanced Light Water Reactors Utility Requirements Document Small Modular Reactors Inclusion Summary," Electric Power Research Institute, Inc., Knoxville, TN (United States), Tech. Rep. 3002003130, Dec. 2014. [Online]. Available: <https://www.osti.gov/biblio/1165570>
- [16] "AP1000 ARIS Specifications." [Online]. Available: <https://aris.iaea.org/PDF/AP1000.pdf>
- [17] "Design Control Document, Revision 15, NRC." [Online]. Available: <https://www.nrc.gov/docs/ML0534/ML053480408.pdf>
- [18] D. Ingersoll, C. Colbert, Z. Houghton, R. Snuggerud, J. Gaston, and M. Empey, "Can Nuclear Power and Renewables be Friends?" in *Proceedings of ICAPP*, vol. 9, 2015, p. 19.
- [19] B. Knueven, J. Ostrowski, and J.-P. Watson, "On Mixed-Integer Programming Formulations for the Unit Commitment Problem," *INFORMS Journal on Computing*, p. ijoc.2019.0944, Jun. 2020. [Online]. Available: <http://pubsonline.informs.org/doi/10.1287/ijoc.2019.0944>
- [20] F. Wang and K. W. Hedman, "Dynamic Reserve Zones for Day-Ahead Unit Commitment With Renewable Resources," *IEEE Transactions on Power Systems*, vol. 30, no. 2, pp. 612–620, Mar. 2015, conference Name: IEEE Transactions on Power Systems. [Online]. Available: <https://ieeexplore.ieee.org/abstract/document/6847237>
- [21] M. Carrion and J. Arroyo, "A computationally efficient mixed-integer linear formulation for the thermal unit commitment problem," *IEEE Transactions on Power Systems*, vol. 21, no. 3, pp. 1371–1378, Aug. 2006. [Online]. Available: <https://ieeexplore.ieee.org/document/1664974>
- [22] "U.S. summer nuclear outages declined in 2024, returning to 2022 levels - U.S. Energy Information Administration (EIA)." [Online]. Available: <https://www.eia.gov/todayinenergy/detail.php?id=63624>
- [23] F. Karg Bulnes, D. Hofer, N. R. Smith, J. Schmitt, O. Pryor, G. Khawly, and A. McClung, "Economic Modeling of Renewable Integration and the Application of Energy Storage to the ERCOT Energy Grid," in *Volume 6: Education; Electric Power; Energy Storage; Fans and Blowers*. London, United Kingdom: American Society of Mechanical Engineers, Jun. 2024, p. V006T08A003. [Online]. Available: <https://asmedigitalcollection.asme.org/GT/proceedings/GT2024/87981/V006T08A003/1204098>
- [24] "Grid Information." [Online]. Available: <https://www.ercot.com/gridinfo>